Topological solitons and dislocations in two- and three-dimensional anisotropic crystals

Christiansen, Peter Leth; Savin, A.V.; Zolotaryuk, Alexander

Published in:
Physical Review B

Link to article, DOI:
10.1103/PhysRevB.57.13564

Publication date:
1998

Document Version
Publisher's PDF, also known as Version of record

Topological solitons and dislocations in two- and three-dimensional anisotropic crystals

P. L. Christiansen
Department of Mathematical Modelling, Technical University of Denmark, DK-2800 Lyngby, Denmark

A. V. Savin
Department of Mathematical Modelling, Technical University of Denmark, DK-2800 Lyngby, Denmark and Institute for Problems of Physics and Technology, 119034 Moscow, Russian Federation

A. V. Zolotaryuk
Department of Mathematical Modelling, Technical University of Denmark, DK-2800 Lyngby, Denmark and Bogolyubov Institute for Theoretical Physics, 252143 Kyiv, Ukraine

(Received 14 November 1997)

The well-known one-dimensional Frenkel-Kontorova model is modified and generalized to describe topological point defects and dislocations in anisotropic crystals of higher dimensions. The main point of our modification is that a substrate periodic potential in the Frenkel-Kontorova model is not considered as a given external spatially periodic force, but it is constructed in a self-consistent manner, such that any disturbance in one of the chains causes a violation of spatial periodicity in the adjacent chains of the crystal. Static and moving soliton (kink and antikink) solutions are found numerically in two- and three-dimensional anisotropic crystals. Bound states of kink-antikink and kink-kink (antikink-antikink) pairs and their dynamical properties are studied. Arrays of soliton states are shown to form dislocations of the edge type and their deformation energy distribution on the crystal lattice is calculated. In finding the soliton profiles and energy distributions on the lattice, we apply the minimization scheme that has proven to be an effective numerical method for seeking solitary wave solutions in complex systems. The collision dynamics of the point defects are also investigated. [S0163-1829(98)02221-8]

I. INTRODUCTION

The well-known one-dimensional (1D) Frenkel-Kontorova (FK) model[1–3] originally introduced for a description of dislocation dynamics in 3D crystals[4,5] has been used extensively for modeling nonlinear dynamical processes in a variety of condensed matter[6,7] and biological[8] systems. As for possible extensions of this model to higher dimensions, so far little work has been done. In this respect, the investigations on the 2D scalar[9–11] and vector[12,13] generalizations of the 1D FK model, including its different quasi-one-dimensional versions,[14–17] which appear to be also complicated systems, should be mentioned. Among these studies, the Lomdahl-Srolovitz 2D generalization[12,13] seems to be the most relative model for a description of dislocation dynamics.

In the theory of dislocations,[4,5] the 1D FK model describes the simplest physical situation when a part of a crystalline material is displaced with respect to another one along a sliding plane. Both these parts, which are separated by the sliding plane, are modeled by chains. The lower chain is considered as a perfect 1D periodic substrate lattice whereas the upper one is assumed to contain a defect, a localized rarefaction (kink), or a localized compression (antikink). However, in realistic crystals, any disturbance in the upper chain (in which the formation of defects is assumed), has obviously an influence on the lower lattice, so that the periodicity of the substrate potential, in general, will be broken. Both the chains should be considered as equivalent objects and the influence of any local stress deformation on the substrate potential should be considered properly. In the present paper, we study an anisotropic crystal consisting of coupled chains that are considered as identical objects, so that any influence of one of the chains on its surrounding chains is taken into account. As in the 2D Pouget lattice model,[18,19] only interatomic forces are included in our model. As a consequence, on-site potentials are not considered at all. Instead, we need to consider long-range interactions between atoms in adjacent chains. The main idea is that because of the shelf in the soft slope of a typical (e.g., Lennard-Jones or Morse) interatomic potential, it is possible to construct numerically an appropriate interchain (substrate) potential in a self-consistent way by summing only a *finite* number of long-range interactions. In order to simplify this numerical scheme, we restrict ourselves in this paper to an anisotropic crystalline material. In this case, it is sufficient to consider only nearest-neighbor harmonic forces along the anisotropy axis and for the construction of a substrate potential we accomplish summation only over the interatomic interactions in adjacent chains of the lattice. For any isotropic crystal, this procedure is more complicated because the summation should be performed also in perpendicular directions.

The paper is organized as follows. In the following section, we present a model in which only interatomic forces are involved. The procedure on how to numerically obtain soliton solutions is described in Sec. III. These solutions are used in Sec. IV to form the initial data for simulations of the equations of motion. The numerical results on the soliton dynamics are also presented in this section. Finally, Sec. V contains a summary and outlook.

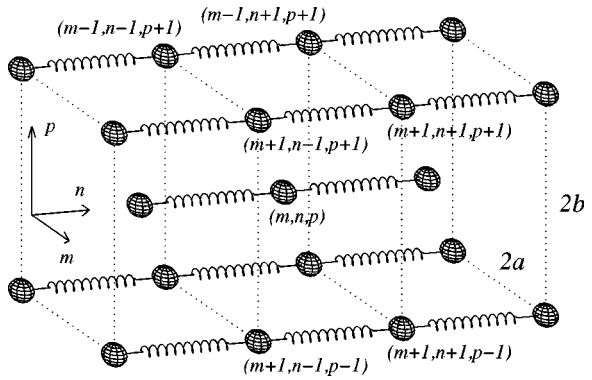

FIG. 1. Schematic representation of the 3D anisotropic crystal structure. Only intrachain bonds are represented (shown by springs).

II. A MODEL

We consider a 3D anisotropic crystal consisting of interacting chains of coupled atoms (or ions) as shown in Fig. 1. Each of these chains is directed along the n axis and the distances between them in the (perpendicular) m and p directions are given by the dimensionless parameters a and b, respectively, (see Fig. 1). The sites of this crystal structure are defined by the following 3D lattice:

$$\Gamma=\{(m,n,p)\in Z^3|\ \text{all}\ \ m,n,p\ \ \text{are either even or odd}\}. \tag{1}$$

For simplicity of numerical calculations as well as for visual purposes, the corresponding 2D version, shown in Fig. 2, is also presented. We consider the simplest (scalar) case when the lattice atoms are constrained to move only in one direction, namely, along the n axis. The intrachain (i.e., interatomic in each chain) forces are considered only between nearest-neighbor atoms whereas the interchain interactions include all the forces corresponding to the potential $V_0(r)$ shown in Fig. 3. But only adjacent chains are considered. In this way, we are able to get a self-consistent substrate potential for each atom in the crystal. When the atoms in adjacent chains are fixed, this potential will be periodic as shown in Fig. 2(c). The interchain potential is constructed by summing its interactions with all of the atoms in the nearest-neighbor chains (two chains in the 2D case or four chains in the 3D case, see Figs. 1 and 2). Therefore, only *interatomic* (both intrachain and interchain) interactions contribute to the total potential energy of the crystal. Next, we assume that the adjacent intrachain interactions are coupled by harmonic forces with some stiffness constant K, whereas the interchain interactions are given by the pair potential $V_0(r)$ with a minimum at $r=r_0$ (see Fig. 3). According to geometry given by Fig. 1, the equilibrium distance r_0 between the nearest atoms from adjacent chains is

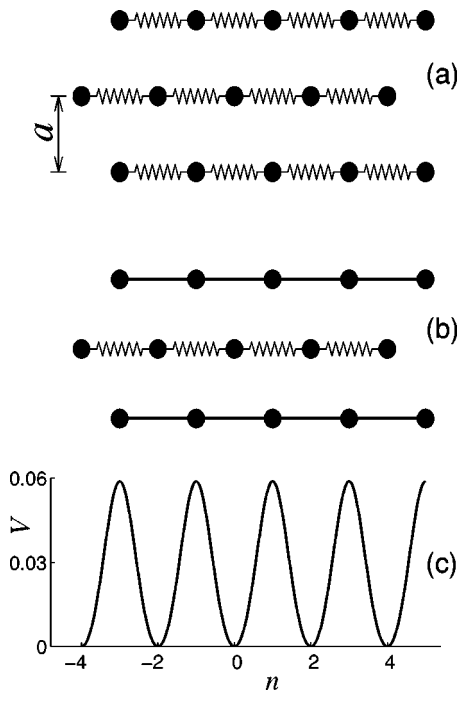

FIG. 2. (a) Schematic representation of the 2D anisotropic crystal structure with only intrachain bonds shown. (b) Single chain with its two adjacent chains, the atoms of which are fixed. (c) On-site potential formed by the adjacent chains with fixed atoms.

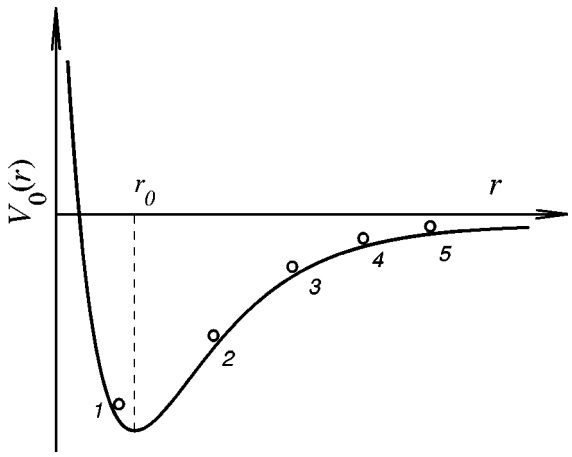

FIG. 3. Positions of the first, second, third, fourth, and fifth neighbors in adjacent chains interacting through the interatomic potential $V_0(r)$.

$$r_0=\sqrt{h^2+1/4},\quad h=\sqrt{a^2+b^2}, \tag{2}$$

if the dimensionless spacing constant along the n axis equals unity. However, the presence of long-range interactions through the potential $V_0(r)$ will reduce the ''bare'' equilibrium distance between the nearest atoms along the n axis (equal to 1) by some value δ because, as shown in Fig. 3, the second, third, and next neighbors are found on the soft slope of the potential $V_0(r)$. The resulting force of these neighbors displaces the first neighbors to the hard slope as shown schematically in Fig. 3. Obviously, this magnitude depends on the form of the potential $V_0(r)$ and in each case it should be determined directly. We normalize the dimensionless potential $V_0(r)$ according to the conditions $V_0''(r_0)=\alpha$ and $V_0(\infty)=0$ where the dimensionless parameter α measures the ratio of the stiffness constant of the interaction between the nearest-neighbor atoms in adjacent chains to the stiffness constant of the interaction between the nearest-neighbor atoms in each chain. The constant α can also be referred to as

the discreetness parameter.[20] Then the reduction constant δ can be found as a solution of the following minimization problem:

$$\delta^2/2+2(D-1)\sum_{j=-\infty}^{\infty} V_0[d_j(\delta)]\rightarrow\min_{\delta}, \tag{3}$$

where D (equal to 2 or 3) denotes the spatial dimension and all the distances between atoms in adjacent chains d_j's depend on δ according to

$$d_j=\sqrt{(j+1/2)^2(1-\delta)^2+h^2}. \tag{4}$$

Here, in the case $D=3$ the parameter h is defined by the second of Eqs. (2) and in the planar case ($D=2$) it equals the distance between adjacent chains a [see Fig. 2(a)].

Summarizing all these arguments, we can write the total energy of such a 3D crystal in the form

$$H=\sum_{(m,n,p)\in\Gamma}\left[\tfrac{1}{2}\dot{u}^2_{mnp}+Kl^2(U_{mnp}+V_{mnp})\right] \tag{5}$$

with K being the intrachain stiffness constant and l the lattice spacing constant. Here u_{mnp} is the dimensionless displacement of the atom located at the (mnp)th lattice site (see Fig. 1) along the n axis from the new equilibrium position in the renormalized lattice and therefore measured in units of $1-\delta$. The first term describes the kinetic energy of atoms while the second and third terms give the total deformation energy of the crystal that consists of the intrachain and interchain interaction energies. Both the intrachain (U_{mnp}) and interchain (V_{mnp}) potential energy densities are taken in a spatially symmetrized form and they are given by the following renormalized expressions:

$$\begin{aligned} U_{mnp}&=U_{mnp}(\delta)\\ &=\tfrac{1}{4}\left[(u_{mnp}-u_{m,n-2,p})^2+(u_{m,n+2,p}-u_{mnp})^2\right] \end{aligned} \tag{6}$$

and

$$V_{mnp}=V_{mnp}(\delta)=\sum_{j=-\infty}^{\infty}\left[\sum_{\nu} V_0(\rho_{\nu jmnp})-4V_0(d_j)\right], \tag{7}$$

where δ is a solution of the minimization problem (3) and the distances $\rho_{\nu jmnp}$'s are defined by

$$\begin{aligned} \rho_{\nu jmnp}&=\rho_{\nu jmnp}(\delta)\\ &\equiv\sqrt{[(j+1/2)(1-\delta)+u_{m\pm1,n+2j+1,p\pm1}-u_{mnp}]^2+h^2}, \end{aligned} \tag{8}$$

where the subscript ν runs over the four values that correspond to the different signs at $m\pm1$ and $p\pm1$, so that $\nu=(+,+),(+,-),(-,+),(-,-)$, summing all the interactions with the four adjacent chains.

For a dimensionless description it is convenient to introduce the dimensionless time and to rescale the spatial variables as follows:

$$\tau=\sqrt{K/m}\,t. \tag{9}$$

The dimensionless Euler-Lagrange equations of motion that correspond to the Hamiltonian given by Eqs. (5)–(8) are obtained in the usual way.

III. SOLITON SOLUTIONS AND POINT DEFECTS

In order to study the equations of motion in a finite domain of the lattice Γ, we need to define the boundary conditions. We choose a 3D rectangle $\Lambda=\{1\leqslant m\leqslant M,\ 1\leqslant n\leqslant N,\ 1\leqslant p\leqslant P\}\subset\Gamma$ and define its interior $I=\{2\leqslant m\leqslant M-1,\ n_0+1\leqslant n\leqslant N-n_0,\ 2\leqslant p\leqslant P-1\}$ where n_0 is some appropriate number that is chosen from the computational point of view; in order to construct the substrate potential, summing the interactions between a given atom and all of the atoms in the adjacent chains, it is sufficient to accomplish the summation over a finite number n_0 of neighbors that depends on the form of the potential $V_0(r)$. Then the boundary of the rectangle Λ is $\partial\Lambda=\Lambda\backslash I$. In other words, besides the boundary chains of the rectangle Λ that cross the (m,p)th plane, the n_0 boundary planes at the left boundary of the rectangle $\partial N_L=\{m,\ 1\leqslant n\leqslant n_0,\ p\}$ and the n_0 boundary planes at the right boundary $\partial N_R=\{m,\ N-n_0+1\leqslant n\leqslant N,\ p\}$ are included into the boundary $\partial\Lambda$. If a soliton (kink or antikink) is found at one of the chains, we call this chain an S chain. Similarly, we define its left and right boundaries as ∂S_L and ∂S_R, respectively.

The kink (antikink) profiles were found by minimization and then were chosen as initial conditions for numerical simulations of the equations of motion that correspond to the Hamiltonian (5)–(8). Afterwards, a final profile of the lattice field $u_{mnp}(\tau)$ under simulations at sufficiently large times τ, allows us to conclude whether or not the initial condition found by the minimization procedure is a correct and stable solution of the equations of motion. The criterion for the method accuracy can be the comparison of a final two-component kink (antikink) profile with the corresponding solution of the minimization procedure when the kink has passed a sufficiently large number of chain sites. Note that we can use for this purpose the cyclic boundary conditions for the lattice field $u_{mnp}(\tau)$. The main point in such a numerical approach is an appropriate choice of a discrete functional (i.e., a function of many variables) for minimization and, as a rule, such a function can be constructed from a corresponding Lagrangian of the system.

Writing the (dimensionless) Lagrangian L that corresponds to the Hamiltonian (5)–(8) and replacing there the time derivative $du_{mnp}/d\tau$ by appropriate spatial difference of the lattice field $u_{mnp}(\tau)$, we can get a function for minimization. Such an approximation can be applied to those lattice functions that (i) are sufficiently smooth from site to site and (ii) have a stationary profile moving with velocity s. To do this, we use the approximation

$$\frac{d}{d\tau}u_{mnp}=-su'(m,n-s\tau,p)\simeq-s(u_{m,n+1,p}-u_{m,n-1,p}). \tag{10}$$

Then the minimization problem can be formulated as follows:

$$-L=\sum_{(m,n,p)\in\Lambda}[(1-s^2)U_{mnp}+V_{mnp}]\rightarrow \min_{\{u_{mnp}|(m,n,p)\in\Lambda\setminus\partial N\}}, \tag{11}$$

where the kink and antikink conditions at the boundary $\partial N=\partial N_L\cup\partial N_R$:

$$u_{mnp}=0 \quad \text{if} \quad (m,n,p)\in\partial N\setminus\partial S_R \quad \text{and}$$

$$u_{mnp}=1 \quad \text{if} \quad (m,n,p)\in\partial S_R \quad (\text{kink}),$$

$$u_{mnp}=1 \quad \text{if} \quad (m,n,p)\in\partial S_L \quad \text{and}$$

$$u_{mnp}=0 \quad \text{if} \quad (m,n,p)\in\partial N\setminus S_L \quad (\text{antikink}), \tag{12}$$

are supposed to be fixed under the minimization process. In order to be certain that the kink solution corresponds to a minimum (or maximum) of the Lagrangian L given by Eq. (11), we accomplish the substitution

$$\frac{d^2}{d\tau^2}u_{mnp}=s^2u''(m,n-s\tau,p)$$

$$\simeq s^2(u_{m,n+2,p}-2u_{mnp}+u_{m,n-2,p}) \tag{13}$$

in the equations of motion and find that the resulting difference equations are nothing more than the extremum conditions $\partial L/\partial u_{mnp}=0$ for all $(m,n,p)\in\Lambda$.

Finally, the dimensionless kink energy E_K, as a function of the dimensionless velocity s, as well as its distribution (i.e., the energy density) E_{mnp} on the lattice domain Λ were calculated according to (compare with the Lagrangian L)

$$E_K=E_K(s)=\sum_{(m,n,p)\in\Lambda}E_{mnp}, \quad E_{mnp}=(1+s^2)U_{mnp}+V_{mnp}. \tag{14}$$

Note that at the boundary chains, the terms U_{mnp} and V_{mnp} in Eqs. (11) and (14) should be redefined properly, taking into account that the interchain interactions exist only from the internal side of the rectangle Λ.

The main part of numerical calculations has been performed for the 2D anisotropic lattice shown in Fig. 2(a) with $\alpha=0.1$. The distances between the atoms in adjacent chains are given by [compare with Eq. (8)]

$$\rho_{\nu jmn}=\sqrt{[(j+\tfrac{1}{2})(1-\delta)+u_{m\pm1,n+2j+1}-u_{mn}]^2+a^2}, \tag{15}$$

where the subscript ν runs over the two signatures $(+)$ and $(-)$. The Morse potential (plotted in Fig. 3)

$$V_0(r)=\frac{\alpha}{\beta^2}\{\tfrac{1}{2}\exp[-2\beta(r-r_0)]-\exp[-\beta(r-r_0)]\} \tag{16}$$

with positive dimensionless constants α and β was used for the construction of the substrate potential.

The solutions of the minimization problem (11) that determine the profiles (i.e., the displacement field u_{mn}) on the 2D lattice for a single kink and a single antikink are presented in Figs. 4(a) and 4(b), respectively. As usual, the soliton solution is referred to as a kink (antikink) if its profile along the n axis is a monotonically increasing (decreasing)

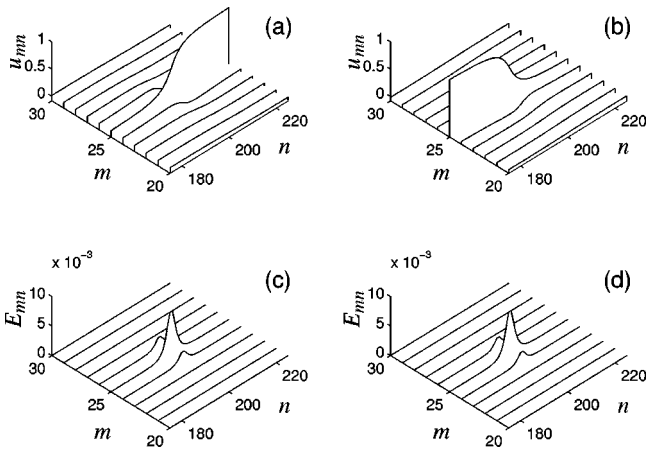

FIG. 4. Single kink and antikink defects: (a) kink and (b) antikink u_{mn} profiles and total energy distribution E_{mn} on the 2D lattice of (c) kink and (d) antikink.

function with the corresponding values 0 or 1 on the boundaries ∂S_L and ∂S_R. The total energy distribution on the 2D lattice E_{mn} is plotted for the kink in Fig. 4(c) and for the antikink in Fig. 4(d). As follows from these figures, the energy of the kink and the antikink is the same and it is distributed not only in the longitudinal n direction, but also along the transverse m axis.

The accuracy of the (moving) kink profiles, found by the minimization procedure and taken to be initial conditions for solving the equations of motion, was examined from their comparison with the final profiles obtained at those times when the kinks have passed a long length (thousands of chain sites). A perfect coincidence of the initial and final profiles was observed. Note that when investigating only wide kinks, we may omit interesting effects due to discreetness.[20,21] In order to treat highly discrete solutions, we should use more complicated numerical techniques such as the pseudospectral method suggested by Eilbeck and Flesch[22] and further developed by Duncan *et al.*[23]

IV. DEFECT DYNAMICS AND DISLOCATIONS

The kink dynamics within one chain does not introduce new effects compared to the 1D theory and the collision dynamics of defects of the same or opposite polarity should have the similar behavior as for the 1D FK model. However, in our case, since kink defects (of the same or opposite polarity) can be found in adjacent chains, the topological situation changes essentially. Thus, defects of opposite polarity being situated in adjacent chains cannot annihilate as in the 1D theory; they form a bound state. Bound states can also be formed by defects of the same polarity. Their energy is distributed along both the m and n directions as illustrated by Fig. 5. Moreover, kinks of the same or opposite polarity can also form a bound state even in the case when they are located not in adjacent chains, but through one (as shown in Fig. 6) or more chains.

By minimization, we have calculated the binding energy of kinks and antikinks (kink-kink, E_{KK}; antikink-antikink, E_{AA}; kink-antikink, E_{KA}) and its dependence on the relative distance between kinks and antikinks $R=|n^c_{m+1}-n^c_m|$, being located in the adjacent mth and $(m+1)$th chains. The posi-

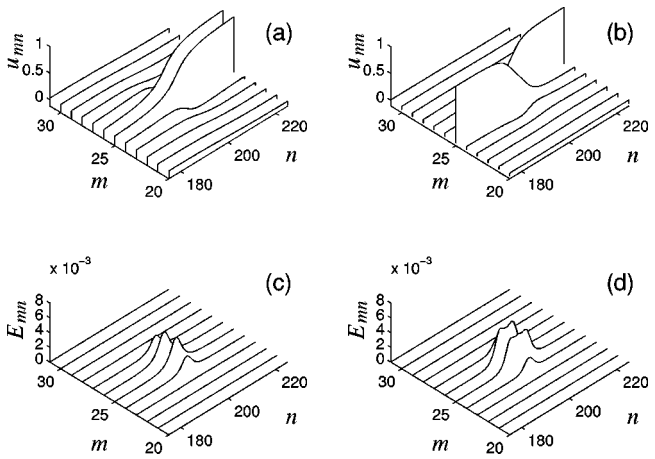

FIG. 5. Bound states of defects of the same and opposite polarity located in adjacent chains: (a) kink-kink and (b) kink-antikink u_{mn} profiles, and energy distribution E_{mn} on the 2D lattice of (c) kink-kink and (d) kink-antikink bound states.

tion of the soliton (kink or antikink) center in the mth chain n_m^c which, in general, depends on time τ, was numerically calculated according to

$$n_m^c = \sum_n n \frac{u_{mn} - u_{m,n-2}}{u_{mN} - u_{m1}}. \tag{17}$$

To calculate each of the binding energies E_{KK}, E_{AA}, or E_{KA}, we solve the minimization problem (11) with the conditions that fix the boundary particles [in both the mth and $(m+1)$th chains] in the corresponding states (for a kink or an antikink). Besides these boundary conditions, we also fix any two nonzero values from the interval of displacements $0<u<1$ (choosing these values close to 1 is more convenient for the procedure), one for some particle in the mth chain and the other for some particle in the $(m+1)$th chain. Having solved the minimization problem (11), according to Eq. (17), we find a certain value for the distance R that appears to be fixed because both the particle displacements are fixed during the minimization procedure. In this way, fitting an appropriate pair of the particles in the mth and the

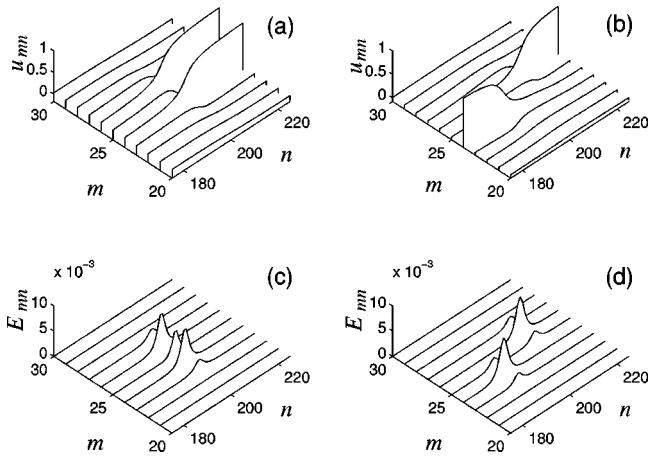

FIG. 6. (a,c) Bound state of two kinks and (b,d) bound state of kink and antikink situated through one chain: (a) kink-kink and (b) kink-antikink u_{mn} profiles and energy distribution E_{mn} of (c) kink-kink and (d) kink-antikink bound states.

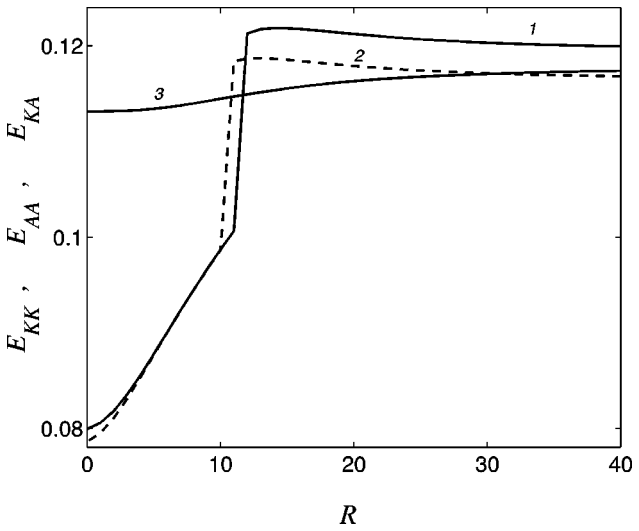

FIG. 7. Total potential energy of the bound states against distance between two kinks (curve 1, solid), two antikinks (curve 2, dashed), and kink and antikink (curve 3, solid).

$(m+1)$th chains, one can get any given distance R and the corresponding interaction energy. The distance between the chosen particles and the fixed values of their displacements uniquely determine the distance R. The relative motion of kinks and antikinks caused by this interaction will be studied below.

As shown in Fig. 7, the behavior of the kink-kink (or antikink-antikink) and kink-antikink interaction energies $E_{KK}(R)$ and $E_{KA}(R)$ essentially differ each from other. Thus, the kink-antikink interaction energy $E_{KA}(R)$ has a behavior similar to the 1D case. It is interesting that the interaction energy of solitons of the same polarity $E_{KK}(R)$ or $E_{AA}(R)$, as illustrated in Fig. 7 by the curves 1 and 2, significantly exceeds the kink-antikink interaction energy E_{KA} for small R, while for large R a repulsion appears in the interaction of solitons of opposite polarity. Note also that since the interatomic interaction potential (16) contains anharmonicity, so that the symmetry between its compression and repulsion parts is broken, the R dependences of E_{KK} and E_{AA} differ slightly each from other.

We have also constructed bound states of several kinks of either the same polarity [see Fig. 8(a,c)] or with the stagger formation [see Fig. 8(b,d)]. As shown in Fig. 8(c), the total deformation energy of a linear array of kinks of the same polarity is concentrated only at the edges of this array; inside it the deformation energy is ''*dissolved*'' around. Contrary, in the case of the stagger arrangement [see Fig. 8(b)], the effect of spreading out the deformation inside the array is absent and the energy is uniformly distributed along the axis of this array as illustrated in Fig. 8(d). Therefore, in the latter case, the solitary plane-wave profile is stable [see Fig. 8(d)], forming a linear defect (dislocation). Note that in the former case of arrays of kinks or antikinks, the degree of the energy dissolution increases with the growth of the array length and this behavior is clearly demonstrated in Fig. 9. The edge dislocation can be constituted from kinks of the same polarity and such a state is presented in Fig. 10 where the Burgers vector **b** is oriented along the n axis. The kink profile has the standard form only in the vicinity of the edge and it com-

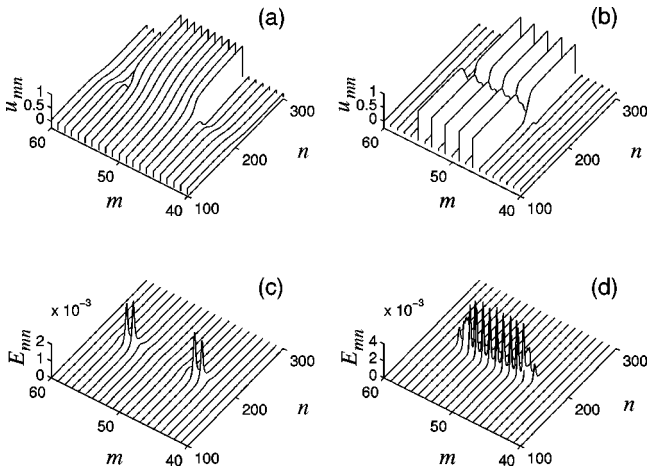

FIG. 8. Linear defects constituted of single kink and antikink defects: the u_{mn} profiles of (a) kink formation and (b) staggered kink-antikink formation and deformation energy distribution E_{mn} of (c) kink and (d) staggered kink-antikink arrangements.

pletely dissolves into the linear slope at the boundary of the lattice domain [see the boundary plot at the 100th chain in Fig. 10(a)]. As shown in Fig. 10(b), the deformation energy is mainly concentrated at the edge.

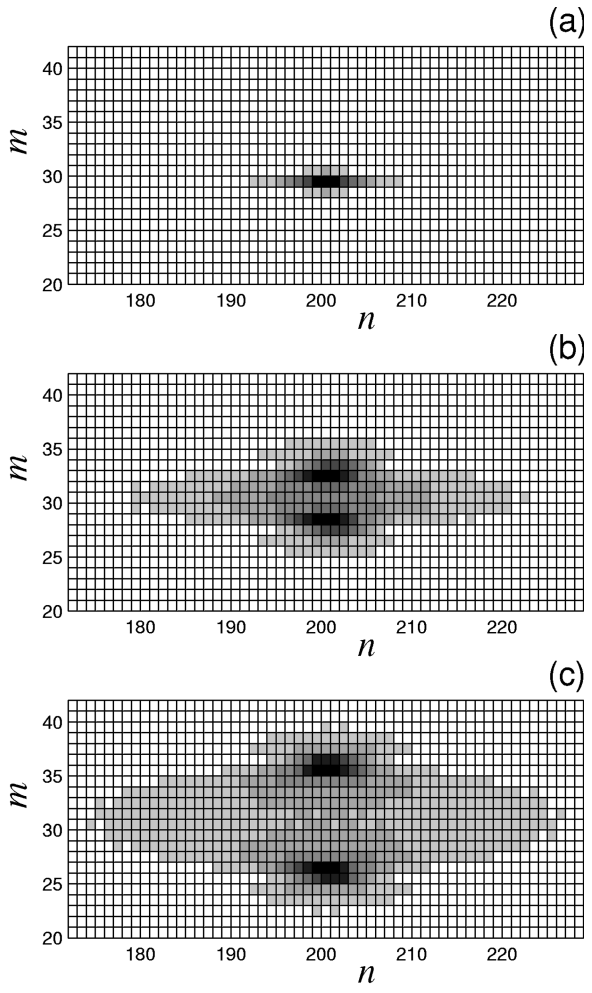

FIG. 9. Energy distribution E_{mn} for (a) single kink, (b) five coupled kinks, and (c) ten coupled kinks on the 2D lattice.

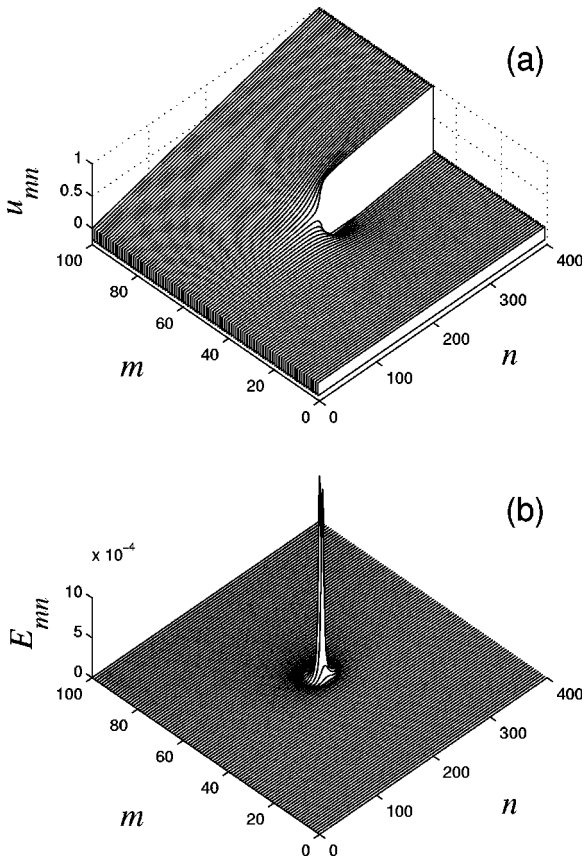

FIG. 10. 2D edge dislocation: (a) displacement profile u_{mn} and (b) energy distribution E_{mn}.

The methods of calculation of the kink energy, kink size, and Peierls-Nabarro relief used previously[24,25] for 1D models can be extended to the present 2D and 3D cases in a straightforward way. Thus, in the mth chain (for the 2D case), the kink width (diameter) is given by

$$D_K = D_K(s) = 2\sqrt{\sum_n (n-n_m^c)^2 (u_{mn}-u_{m,n-2})/(u_{mN}-u_{m1})}, \tag{18}$$

where the kink center n_m^c is given by Eq. (17). In order to examine the effects of our self-consistent approach, we also calculated the parameters for a kink in one S chain when atoms in its adjacent chains were fixed (i.e., the standard 1D FK chain). For the 2D lattice the results of numerical calculations of the kink parameters in the two cases (atoms in the two adjacent chains are mobile and immobile) are presented in Figs. 11 and 12. Thus, Fig. 11 describes the dependence of the kink width D_K and the PN barrier height ΔE on the relative magnitude of the intrachain and interchain stiffness constants given by the parameter α. We observe that the width of the kink profile in the 2D case significantly exceeds that in the 1D case, when atoms in the adjacent chains are fixed as illustrated by Fig. 11(a). In spite of this, the PN barrier is *higher* in the former case [compare the curves 3 and 4 in Fig. 11(a)]. This unexpected result is due to the self-consistency of the interchain interaction. Due to this interaction the kink energy is dissolved, so that its propagation

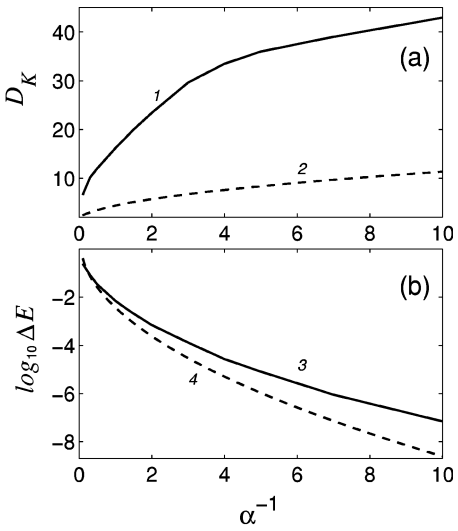

FIG. 11. (a) Kink width D_K and (b) decimal logarithm of the PN barrier height ΔE against α^{-1}. The case when atoms in adjacent chains are allowed to move is represented by solid curves 1 and 3 and the dashed curves 2 and 4 describe the situation when atoms in adjacent chains are fixed.

becomes more difficult, despite it is of larger radius. The energy and width of a kink against its velocity s are plotted in Fig. 12. Here we have found a behavior similar to the 1D FK model.

The results presented in Fig. 7 predict the collision processes of kinks and antikinks. The results of such collisions are presented in Fig. 13(a,b,c) for the kink-kink interaction

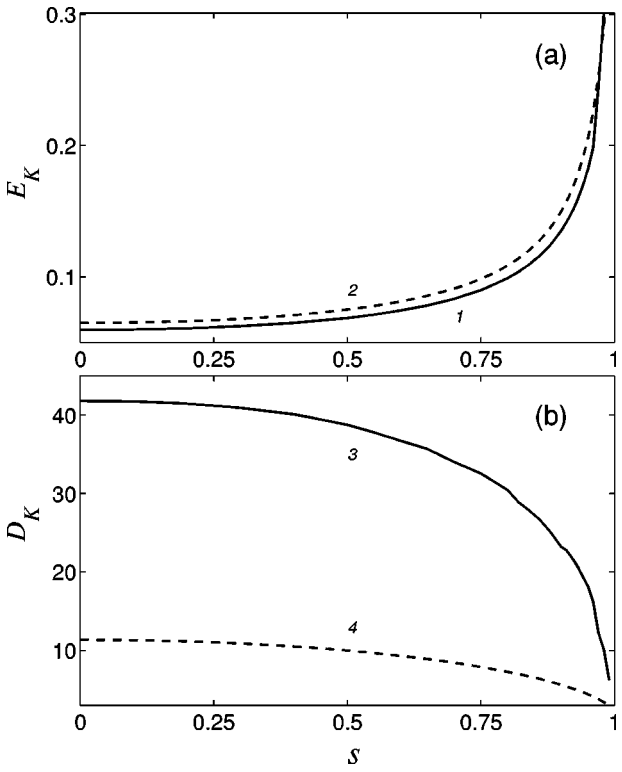

FIG. 12. (a) Kink energy E_K and (b) kink width D_K against kink velocity s for two cases: atoms in adjacent chains are allowed to move (solid curves 1 and 3) and atoms in adjacent chains are fixed (dashed curves 2 and 4).

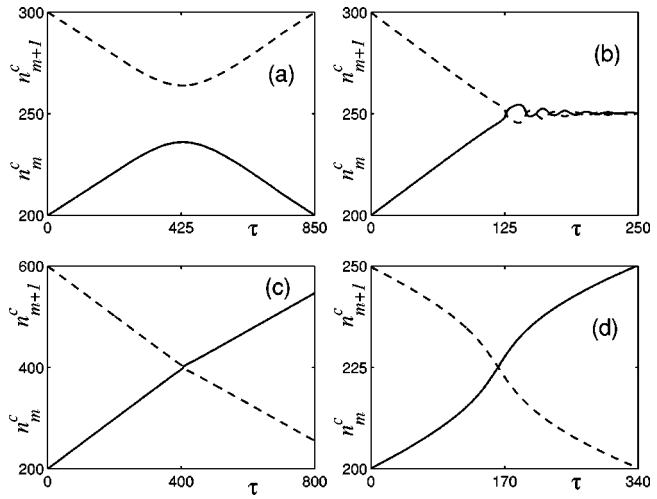

FIG. 13. Kink-kink and kink-antikink collisions with initially given different velocities: (a) reflection of kinks at small velocities ($s=0.1$), (b) kink-kink coupling at larger velocities ($s=0.4$), (c) passage of kinks through each other ($s=0.5$), and (d) kink-antikink collision ($s=0.1$). The solid curves represent the trajectories of one kink located in the mth chain and the dashed lines the trajectories of the other kink or the antikink located in the $(m+1)$th chain.

and in Fig. 13(d) for the kink-antikink interaction. Due to the repulsive part in the kink-kink (or antikink-antikink) interaction shown in Fig. 7 by the curve 1 (or 2), the reflection of kinks each from other occurs [see Fig. 13(a)]. However, if the kinks collide with higher incoming velocities, the activation barrier in the energy E_{KK} (see the curves 1 and 2 in Fig. 7) can be overcome, resulting in a coupled state as shown in Fig. 13(b). The further increase of the incoming velocities leads to passage of the kinks through each other. As for the kink-antikink collision, due to the interaction given by the curve 3 in Fig. 7, a kink and an antikink always pass through each other as shown in Fig. 13(d).

The results of numerical studies for the 3D lattice are presented in Fig. 14. We have found the kink solutions in (a) a single S chain, (b) several S chains staggering to form a 2D stripe, and (c) several stripes of S chains staggering in a 3D rectangle. The deformation energy per one S chain $\overline{E}_{mp}=\Sigma_n E_{mnp}$ is plotted in Fig. 14. These defects can be classified as follows: a *point* (elementary) defect, and *linear* and *plane* defects constituted from the elementary defects. Since the 3D lattice is a realistic case for dislocation patterns, we may describe the array of solitons represented by Fig. 14(c) as an *edge* dislocation. The closed rectangle dislocation line passes along the maximum of the deformation energy and the Burgers vector **b** is oriented along the n axis.

V. SUMMARY AND OUTLOOK

There is still a little progress in realistic generalizations of the standard 1D Frenkel-Kontorova (FK) model that was originally suggested to describe dislocations in 3D crystals. Among the work[9–13] in this direction, the Lomdahl-Srolovitz model seems to be the most realistic. In the present paper, we attempted to attack this problem by constructing a substrate

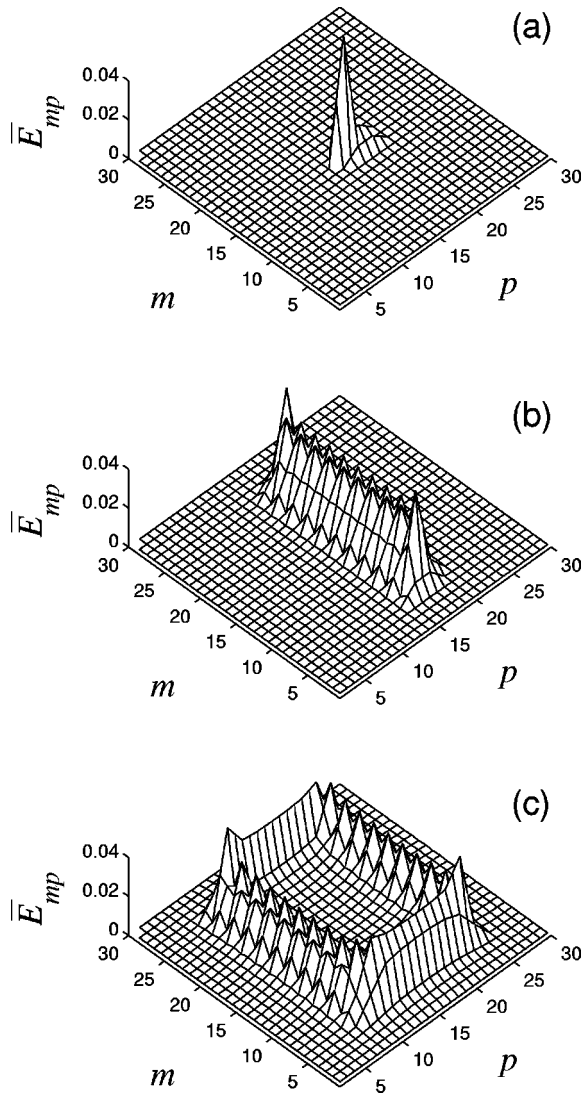

FIG. 14. Energy distribution per one chain $\overline{E}_{mp}$ [in the (m,p) plane of the 3D lattice] for (a) single kink, (b) 1D array of (20) coupled kinks, and (c) 2D array of (20×15) coupled kinks.

potential that is not given as an external source; instead, all the chains of crystal structure without any exception are considered equally and a defect may be considered in any of them. The main reason for adopting this point of view is as follows: since any distortion of an atom in one of the chains (subjected to the adjacent chains) makes obviously an influence on its surrounding atoms, the on-site potential used as a basic point in the FK theory cannot be assumed anymore as a strictly given periodic function. Instead of the periodic substrate potential, a deformable potential that is sensitive to displacements of atoms in adjacent chains should be involved. Such a substrate potential will be a periodic function only in the case if the arrangement of all atoms in the adjacent chains is fixed. Clearly, the periodicity will be broken if the atoms are allowed to move. Therefore we give up from the standard approach when some effective external periodic substrate (on-site) potential is a necessary ingredient of the theory. Contrary, we deal only with *interatomic* interactions and long-range forces must be considered in our approach to construct properly an interchain substrate potential. Moreover, such an approach can be accomplished only if, at least, two dimensions are involved into consideration, so that it is necessary to consider a lattice of two or three dimensions. It is impossible to develop our scheme in the frame of a 1D chain. In the simplest case, an anisotropic 2D crystal consisting of arrays of interacting chains of harmonically coupled particles may be considered.

Our approach of constructing a substrate potential by using a pair interatomic potential seems to be very promising in treating *vector isotropic* models as well. We believe that in such a way one can obtain topological isotropic solitons on a 3D lattice. These objects would not be in contradiction with the Derrick theorem[27,28] because in the continuum limit they become generalized functions[26] as can be easily seen from Figs. 4–6, 8, and 10 of this paper. Thus, the kink (antikink) solution which describes a point topological defect (see Fig. 4) becomes a δ-distributed (along the transverse m axis) function in the continuum limit. Nevertheless, solutions analyzed here might be of interest from the point of view of families of 3D solitons studied in the field theory, for instance, in the problem of the classical 't Hooft-Polyakov monopole[29] and its quantum relatives.[30]

The quasi-one-dimensional model suggested and studied in this paper is interesting from the point of view of the dynamics of topological solitons. Since the total deformation energy of a single defect is also distributed transverse directions, kinks and antikinks can interact even being in different (adjacent) chains, forming coupled states. Because of topological reasons they obviously cannot annihilate, even they are of opposite polarity. On the other hand, kinks or antikinks of the same polarity being placed in adjacent chains can be coupled as well. It is interesting that the coupling in the latter case exceeds that of kink-antikink pairs. The next important result is that the deformation energy of an array of coupled kinks or antikinks is mainly focused at the array edges. In the interior surrounded by these edges, the deformation energy dissolves and the area of this region is enlarged with the growth of the total number of the point (elementary) defects. This set of all the elementary defects can be identified with a dislocation that in our case is of the *edge* type because the Burgers vector **b** is oriented perpendicularly to the line linking all the edges (called a dislocation line).

One should emphasize that any straightforward generalization of the 1D FK model, using a local (on-site) potential cannot satisfactorily describe the point defects. Thus, the 2D versions suggested and studied previously cannot be used for these purposes. For instance, compared with the 2D model studied by Pouget *et al.*,[10] our model is discrete in the transverse direction as well because we consider lattices consisting of arrays of chains. In order to have the displacive limit in the longitudinal direction, we need to have sufficiently strong stiffness along this direction rather than in the perpendicular one. The Lomdahl-Srolovitz model[12,13] also does not allow us to consider point defects. However, domain walls and edge dislocations can be constructed in the frame of our model as arrays of point defects. The dynamics and structure of such domain walls was shown to be interesting and unexpected results on their dynamics have been obtained. It was shown that the domain wall constructed from the point defects has nonuniform deformation energy distribution, while the domain wall consisting of a stagger arrangement of kinks

and antikinks has the straight line configuration with an uniform energy distribution along the line. Our microscopic model does not contain noncentral or bending interactions and therefore on its basis we cannot constitute screw dislocations (for which the Burgers vector **b** is parallel with a dislocation line) from the elementary defects. For these purposes the present model should be generalized to include such interactions. The work in this direction is in progress.

ACKNOWLEDGMENTS

This work was partially carried out with the financial support from the European Economic Community (EEC) under the INTAS Grant No. 96-158. Both of us (A.V.S. and A.V.Z.) would also like to express our gratitude to the MIDIT Center and the Department of Mathematical Modelling of the Technical University of Denmark for financial support and hospitality.

[1] J. Frenkel and T. Kontorova, Phys. Z. Sowjetunion **13**, 1 (1938).
[2] F. C. Frank and J. H. van der Merwe, Proc. R. Soc. London, Ser. A **198**, 205 (1949).
[3] For a review, see, e.g., A. M. Kosevich, *Physical Mechanics of Realistic Crystals* (Naukova Dumka, Kyiv, 1981).
[4] See, e.g., A. H. Cottrell, *Theory of Crystal Dislocation* (Blackie, London, 1964).
[5] J. P. Hirth and J. Lothe, *Theory of Dislocations* (Wiley, New York, 1968).
[6] S. Aubry, in *Solitons in Condensed Matter Physics*, edited by A. R. Bishop and T. Schneider (Springer, Berlin, 1978), p. 264.
[7] A. R. Bishop, J. A. Krumhansl, and S. E. Trullinger, Physica D **1**, 1 (1980).
[8] For a review, see, e.g., L. V. Yakushevich, Physica D **79**, 77 (1994).
[9] W. T. Sanders, J. Appl. Phys. **36**, 2822 (1965).
[10] J. Pouget, S. Aubry, A. R. Bishop, and P. S. Lomdahl, Phys. Rev. B **39**, 9500 (1989).
[11] J. M. Tamga, M. Remoissenet, and J. Pouget, Phys. Rev. Lett. **75**, 357 (1995).
[12] P. S. Lomdahl and D. J. Srolovitz, Phys. Rev. Lett. **57**, 2702 (1986).
[13] D. J. Srolovitz and P. S. Lomdahl, Physica D **23**, 402 (1986).
[14] O. M. Braun and Yu. S. Kivshar, Phys. Rev. B **44**, 7694 (1991).
[15] O. M. Braun, O. A. Chubykalo, Yu. S. Kivshar, and L. Vázquez, Phys. Rev. B **48**, 3734 (1993).
[16] P. L. Christiansen, A. V. Savin, and A. V. Zolotaryuk, Phys. Rev. B **54**, 12 892 (1996).
[17] P. L. Christiansen, A. V. Savin, and A. V. Zolotaryuk, J. Comput. Phys. **134**, 108 (1997).
[18] J. Pouget, Phys. Rev. B **43**, 3575 (1991).
[19] J. Pouget, Phys. Rev. B **46**, 10 554 (1992).
[20] M. Peyrard and M. D. Kruskal, Physica D **14**, 88 (1984).
[21] Y. Zolotaryuk, J. C. Eilbeck, and A. V. Savin, Physica D **108**, 81 (1997).
[22] J. C. Eilbeck and R. Flesch, Phys. Lett. A **149**, 200 (1990).
[23] D. B. Duncan, J. C. Eilbeck, H. Feddersen, and J. A. D. Wattis, Physica D **68**, 1 (1993).
[24] M. Peyrard and M. Remoissenet, Phys. Rev. B **26**, 2886 (1982).
[25] St. Pnevmatikos, A. V. Savin, A. V. Zolotaryuk, Yu. S. Kivshar, and M. J. Velgakis, Phys. Rev. A **43**, 5518 (1991).
[26] I. M. Gelfand and G. E. Shilov, *Generalized Functions, Part 1: Properties and Operations* (Academic, New York, 1964).
[27] R. Rajaraman, *Solitons and Instantons* (North-Holland, Amsterdam, 1982).
[28] G. H. Derrick, J. Math. Phys. **5**, 1252 (1964).
[29] G. 't Hooft, Nucl. Phys. B **79**, 276 (1974); A. M. Polyakov, Zh. Eksp. Teor. Fiz. Pis'ma Red. **20**, 430 (1974) [JETP Lett. **20**, 194 (1974)].
[30] H. Flyvbjerg, Nucl. Phys. B **184**, 351 (1981).